Multipeak-structured photoluminescence mechanisms of as-prepared and oxidized Si nanoporous pillar arrays*

Xu Hai-Jun(许海军)†, Chan Yu-Fei(廛宇飞), and Su Lei(苏 雷)

State Key Laboratory of Chemical Resource Engineering and School of Science, Beijing University of Chemical Technology, Beijing 100029, *China*

(Received 10 May 2011; revised manuscript received 8 June 2011)

Silicon dominates the electronic industry, but its poor optical properties mean that it is not preferred for photonic applications. Visible photoluminescence (PL) was observed from porous Si at room temperature in 1990, but the origin of these light emissions is still not fully understood. This paper reports that an Si nanocrystal, silicon nanoporous pillar array (Si-NPA) with strong visible PL has been prepared on a Si wafer substrate by the hydrothermal etching method. After annealing in O_2 atmosphere, the hydride coverage of the Si pillar internal surface is replaced by an oxide layer, which comprises of a great quantity of Si nanocrystal (nc-Si) particles and each of them are encapsulated by an Si oxide layer. Meanwhile a transition from efficient triple-peak PL bands from blue to red before annealing to strong double-peak blue PL bands after annealing is observed. Comparison of the structural, absorption and luminescence characteristics of the as-prepared and oxidized samples provides evidence for two competitive transition processes, the band-to-band recombination of the quantum confinement effect of nc-Si and the radiative recombination of excitons from the luminescent centres located at the surface of nc-Si units or in the Si oxide layers that cover the nc-Si units because of the different oxidation degrees. The sizes of nc-Si and the quality of the Si oxide surface are two major factors affecting two competitive processes. The smaller the size of nc-Si is and the stronger the oxidation degree of Si oxide layer is, the more beneficial for the luminescent centre recombination process to surpass the quantum confinement process is. The clarification on the origin of the photons may be important for the Si nanoporous pillar array to control both the PL band positions and the relative intensities according to future device requirements and further fabrication of optoelectronic nanodevices.

Keywords: silicon nanocrystal, photoluminescence, annealing effect, quantum confinement, luminescent centre

PACS: 78.55.–m, 78.67.–n, 78.66.–w **DOI:** 10.1088/1674-1056/20/10/107801

1. Introduction

The great success of the microelectronic industry is mainly based on Si and its oxide, which have excellent properties for microelectronic devices. However, bulk Si is inefficient as a light source due to its indirect energy band gap. This has given the information age a 'split personality' in which digital data processing is performed by Si electronics,[1] but increasingly vast amounts of data is transferred optically by using photons generated and detected by III–V semiconductors. This problem is likely to become more acute in the future as the information technology industry moves to optical interconnects for board-to-board and chip-to-chip communications. Since visible photoluminescence (PL) was observed in porous Si (PS),[2] various low-dimensional luminescence Si nanostructures, such as PS,[2−6] large area PS nanowire array,[7] Si nanoparticles,[8] Si quantum dots,[9] and Si nanowire[10] have attracted great interest due to their exhibitions of visible luminescence and the realization of Si-based light emitting devices which are compatible with current electronic ultra-large-scale-integration technologies. Therefore, various Si nanostructures have been synthesized by using several techniques, such as the electrochemical etching method,[2−6] hot-filament chemical vapour deposition (HFCVD),[11] the metal/SiO_2 assistant dry-etching[12], the hydrothermal etching method,[13,14] etc. Among these synthesized methods, the hydrothermal etching method is very significative not only for producing large area regular Si nanocrystal (nc-Si) materials, but also to easily obtain uniform nc-Si layers on the positive and negative surfaces of Si wafers.[13,14]

Although researchers have extensively carried out

*Project supported by the Doctoral Fund of the Ministry of Education of China (Grant No. 20090010120014), the Beijing Natural Science Foundation (Grant No. 1103033), and the Fundamental Research Funds for the Central Universities.

†Corresponding author. E-mail: hjxu@mail.buct.edu.cn

© 2011 Chinese Physical Society and IOP Publishing Ltd

studies on the luminescence behaviours of PS,[1,15,16] nc-Si/SiO_2 film,[17] natively (or thermally) oxidized Si nanostructures,[18] and self-ion-implanted Si-on-insulator structure[19] for more than a decade, the mechanism of the light emission from these nc-Si materials is not fully understood and still causes controversy. Some work suggests that the light emission is due to radiative recombination occurring at the defect states localized at the surface of the nc-Si core or extrinsic centres,[9,20,21] others widely use quantum confinement (QC) effect theory to ascribe the highly efficient light emission via the band-to-band radiative recombination of electron–hole pairs confined within nc-Si.[1,22] Recently, based on the fact that about 1%–2% oxygen atoms would be present in the as-prepared nc-Si surface after 30 min exposure in air and the quantitative discrepancy between the PL peak energy and the band gap energy in the QC theory,[9,23] a new "mixed" model, the quantum confinement-luminescence centre (QCLC) mode, was proposed.[24] In this model, the photoexcitation of electron–hole pairs occurs mainly in the nc-Si core, while most of the photoexcited electrons and holes tunnel in the luminescence centres (LCs) in the surrounding Si oxide layers and recombine there.[24] Although it seems difficult to contrive a unified model that can explain the physical mechanism of light emission, clarification of the origin of the light emission in low-dimensional Si nanostructures might be important for controlling both the position and the relative intensity of the PL bands according to future Si-based light emitting device requirements.

In this work, we are concerned with the strong visible luminescence behaviours of an nc-Si system, Si nanoporous pillar array (Si-NPA), which is prepared by the hydrothermal etching method and has a unique Si hierarchical structure, by investigating contrastively the changes of the bonding configurations and the chemical compositions before and after the thermal oxidization. The annealing processes of the fresh samples are carried out under optimized conditions, which leads to the photoluminescence (PL) intensity in the oxidized Si-NPAs being more stable. In fact, the physically absorbed oxygen at the internal surface of the nanopores may attack Si–Si or Si–H back bonds forming an Si–O–Si bridge during the annealing process. Efficient triple-peak PL from blue to red before annealing and strong double-peak blue PL after annealing were observed for Si-NPAs, and correspondingly the physical mechanisms of light emission are discussed in detail.

2. Experiments

The Si–NPAs were prepared by hydrothermally etching (111)-oriented, boron-doped single crystal Si wafers in a solution of hydrofluoric acid containing ferric nitrate.[14] Here, the Si wafer with a resistivity of $10^{-3}\ \Omega\cdot\mathrm{cm}\sim10^{-2}\ \Omega\cdot\mathrm{cm}$ and hydrothermal treatment at 170 °C for 10 min were adopted to obtain the strong luminescence Si-NPA samples. After the etching process, the obtained samples were copiously rinsed in de-ionized water and dried at room temperature. The thermal annealing process was performed in a tube furnace in dry, flowing oxygen gas at 700 °C for 30 min (an optimized condition) and we named it "annealed Si-NPA". The morphology and microstructures of two samples were characterized by field emission scanning electron microscopy (FE-SEM) (JEOL JSM-6700F), a tunneling electron microscope (TEM) and high resolution TEM (HRTEM) (Philips CM 200 FEG). The elemental compositions as well as the chemical valence states of the surface layers of the Si-NPAs were investigated by X-ray diffractometry (XRD) with Cu K_α radiation (35 keV, 30 mA), Fourier-transform infrared transmission measurements (FTIR, Perkin Elmer, Paragon 1000, MAGNA-IR 750 Fourier-transform spectrometer) and X-ray photoelectron spectroscopy (XPS) (Axis Ultra, Kratos). The PL spectra were recorded at room temperature for all samples by using an SPEX SPEXF212 fluorescence spectrometer, an xenon lamp served as the source of continuous radiation.

3. Results and discussion

The Si-NPA could be well described as a micron/nanometer structural composite system characterized by a hierarchical structure.[14] A regular array is composed of micron-sized, quasi-identical Si pillars, with nanopores densely packed on each Si pillar and beneath the transitional porous layer, and nc-Si forming the pore walls and also encapsulated by SiO_x shells. Detailedly, the regular Si pillars had a density of $1.1\times10^7\ \mathrm{cm}^{-2}$, a height of ∼4.1 μm and a top–top distance of ∼3.6 μm (Fig. 1(a)), nanopores decreased in size gradually from top to bottom (∼40 nm at the pillar tops and ∼15 nm at the pillar roots) and were densely distributed on each silicon pillar, smaller-sized

nanopores with an average size of ∼8.2 nm also existed beneath transitional porous layer, and nc-Si with the sizes from ∼1.95 nm to ∼4.4 nm (an average size of ∼3.4 nm) and a planar density of $\sim 2.3 \times 10^{12}$ cm^{-2} formed each nanopore wall.[14] After annealing for 30 min at 700 °C, just as shown in Fig. 1(b), it can be found that there are no differences in the micrometer Si pillars for annealed Si-NPA as compared to the as-prepared Si-NPAs. Figures 1(c) and 1(d) present the typical HRTEM images of the pore walls of the as-prepared and annealed Si-NPA, where uniformly distributed nc-Si crystal zones were observed and the average nc-Si sizes were estimated as ∼3.4 nm and ∼3.0 nm, respectively. Clearly, the average sizes of the basic units, nc-Si, become smaller after being annealed, which is different from that of the almost unchanged micron Si pillars.

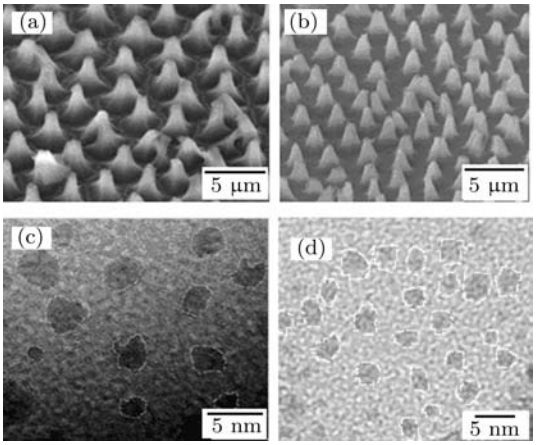


Fig. 1. The FE-SEM micrographs of (a) Si-NPA and (b) annealed Si-NPA. Both the images were taken with the samples being titled at an angle of 40°. Panels (c) and (d) are HRTEM images of the pore walls of the Si-NPA and the annealed Si-NPA, respectively.

Figure 2 shows XRD profiles of two samples. The diffraction line of annealed Si-NPA is composed of one diffuse pattern and that of as-prepared Si-NPA is a sharp one. The nc-Si average sizes can be estimated by using the Scherrer equation:[24] $\tau = K\lambda/\beta_\tau \cos\theta$, where K is the shape factor of a value of 0.9, λ is the wavelength of the incident X-ray and β_τ is given by $(B^2–b^2)$ in radian units where B is the width at half maximum of the diffraction peak and b is the diffraction peak width of the corresponding bulk material. When the Si (111) diffraction peaks at 28.5° in Fig. 2 are chosen for the calculation, the average crystallite sizes of ∼3.8 nm and ∼2.8 nm for Si-NPA and annealed Si-NPA are obtained, respectively. It is clearly shown that the nc-Si sizes of Si-NPA decrease due to their surface oxide of nc-Si with the annealing effect, which would influence their optical properties because of quantum confinement effect of nc-Si. This estimated result of nc-Si sizes is accordant with that of the observed HRTEM images.

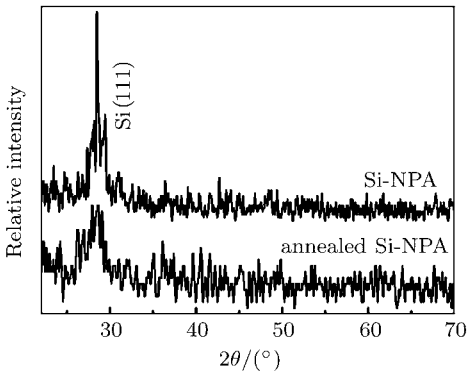


Fig. 2. The XRD patterns of Si-NPA and annealed Si-NPA.

Table 1. Two-peak fitting of the Si–O–Si absorption signal around 1100 cm^{-1} for Si-NPA (A) and annealed Si-NPA (B). Fitting values are peak position (cm^{-1}) and full width at half maximum (FWHM) (cm^{-1}) of both AS_1 and AS_2 peaks.

	TO for AS_1		TO of AS_2	
Samples	Position	FWHM	Position	FWHM
A	1060	75	1143	85
B	1071	85	1190	40

In an attempt to understand the effect of annealed oxidation, the background corrected FTIR absorption spectra of Si-NPA and the annealed one were collected in the 800 cm^{-1}–1500 cm^{-1} region and are shown in Fig. 3. All of the samples were analysed after about three weeks of storage in clean and dry ambient atmosphere following preparation or annealing. The clearly pronounced IR bands peaked at ∼930, ∼980 and ∼1060 cm^{-1} are characteristic for Si-NPAs and only ∼1070 cm^{-1} band for annealed Si-NPA. The ∼930-cm^{-1} and ∼980-cm^{-1} absorption bands are Si–H_x scissor modes and are almost removed from the annealed sample. Considering that ∼1%–2% oxygen atoms are present in the porous Si layer after 30 min air exposure,[23] we find that the as-prepared Si-NPAs studied here is also naturally oxidized and the ∼1060 cm^{-1} absorption peak reflects the state of the natural oxide on its surface. Just as discussed previously,[15] almost all of hte absorption signals in the region of 1050 cm^{-1}–1200 cm^{-1}, which are attributed to the asymmetric stretching (AS) of Si–O–Si bridges, could be split into two peaks, as shown in Fig. 3. Actually, the studies of the vibrational modes of Si–O–Si in oxidized nc-Si systems have pointed

out that these two peaks are the result of two vibrational modes.[15,26] In one mode, AS_1, adjacent oxygen atoms execute the AS motion in phase with each other and, in the other mode, AS_2, adjacent oxygen atoms execute the AS motion 180° out of phase. It proposes that the transverse-optic (TO) of the AS_1 mode is centred at ∼1080 cm^{-1}, while the TO of the AS_2 mode is ∼1200 cm^{-1}.[26,27] The least-square method is used here and Table 1 shows the fitting values of two Si–O–Si absorption peaks. It can be concluded that the weight of the AS_1 mode increased from Si-NPA to an oxidized one accompanying with the decrease of the weight of AS_2, and the weight of AS_1 strength of the annealed Si-NPA was notably larger than that of the as-prepared Si-NPA. According to Li's study of the above two Si–O–Si peaks in a structural investigation of annealed PS, we believed that the increase of the FWHM of the lower wave-number peak at ∼1100 cm^{-1} after heat-treatment was due to the decrease of the disorder level, the amorphous level and strain in the surface layer.[15] The FTIR results of our samples reveal that, after annealing, the disorder level, amorphous level and strain of the oxide layer decrease and the quality of the oxidized surface improves in annealed Si-NPA. Actually, with reference to the XPS experimental results, we estimate the thicknesses of SiO_x films on the surface at ∼1.32 nm and ∼1.79 nm for Si-NPA and annealed Si-NPA,[14] respectively, this also proves the conclusions that the quality of the oxidized surface improves after annealing.

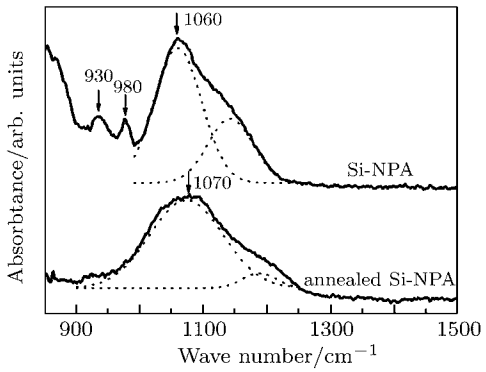


Fig. 3. The FTIR absorption spectra of the Si-NPA and the annealed Si-NPA. The dotted lines are the fitting spectra of the Si–O–Si asymmetric stretching mode around 1100 cm^{-1}.

Figure 4(a) shows the room temperature PL spectra taken from the Si-NPA and the annealed Si-NPA under the 350-nm ultraviolet irradiation, which is the most effective excitation wavelength (EW). All PL measurements were carried out under the same conditions. The PL spectrum of the Si-NPA has three emission bands, one in the blue light range and the others in the red range, which construct a triple-band spectral structure. Fitting the spectrum by Gauss method, we can determine the peak positions of three emission bands and decompose it into three separated emission bands, peaked at ∼418 nm, ∼640 nm, and ∼705 nm, respectively. After annealing at 700 °C for 30 min and at the same 350-nm ultraviolet irradiation , the triple-band spectral structure of PL turns into a double-band spectral structure (Fig. 4(a)), which shows that the two red PL bands of Si-NPA disappear and another blue PL band near ∼465 nm appears. At the same time, the PL intensity of the annealed Si-NPA decreases. Comparing the peak positions and shapes with that of the Si-NPA, it is suggests that the ∼420 nm and ∼465 nm blue PL bands are observed possibly due to the annealing effect. In Fig. 4(a), the intensities of two red PL bands are stronger than those of the blue band for the Si-NPA and this phenomenon could be also observed from the direct fluorescence microscopy image of the Si-NPA layer excited by 325-nm laser radiation, as shown in Fig. 4(b). Correspondingly, the strong blue fluorescence microscopy image of the annealed Si-NPA layer is also observed from Fig. 4(c). The time evolutions of the PL spectra of the Si-NPA and the annealed Si-NPA were also carried out. After one year following their preparation, both the peak intensities and the positions of all PL bands for two samples under identical EW remain nearly unchanged.

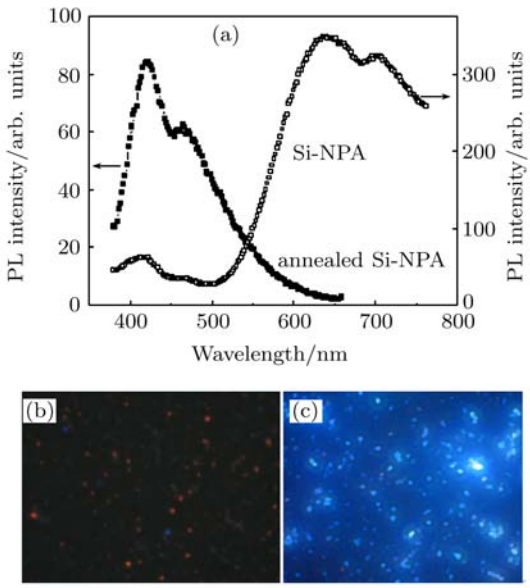


Fig. 4. (a) Room-temperature PL spectra of the Si-NPA and the annealed Si-NPA excited by 350-nm ultraviolet radiation. The fluorescence microscopy images of as-prepared Si-NPA layer (b) and annealed Si-NPA layer (c) excited by 325-nm laser radiation.

The origin of the three emission bands of the as-prepared Si-NPA can be well explained by the co-existence of the QC and QCLC processes. The excitation process for the three emission bands are identical, which occurs in nc-Si through a carrier band–band transition process. The recombination paths are different for the three emission bands, the blue PL band originates from the band–band recombination and the two red PL bands originate from two kinds of LC-band recombination. Here, some experimental facts for explaining the PL mechanism of the Si-NPA, which could be well explained by the co-existence of the QC process and QCLC process rather than by the single QC, QCLC or other models, are given below.

(i) Setting the monitoring wavelength at 420, 640 and 705 nm, respectively, we find that all the three PL excitation (PLE) spectra exhibit the same peak pinned at ∼365 nm, as shown in Fig. 5(a). This indicates that the most effective excitation wavelength (EW) for all the three emission bands is the same one and strongly suggests that the excitation process for them might be identical. Based on the research result of the PL mechanism of various Si nanostructures,[24] the PLE process in the Si-NPA should be attributed to a band–band transition of carriers in nc-Si.

(ii) The peak intensities of the ∼418 nm blue PL band decrease monotonously and the full width at half maximum (FWHM) narrows continuously with the change of EW from 340 nm to 430 nm, while the PL peak position increases monotonously with EW (Fig. 6(a)). When EW was changed from 340 nm to 430 nm, a red shift of ∼60 nm of the peak position was observed, from ∼418 nm to ∼480 nm. Such a strong emission–excitation depen-

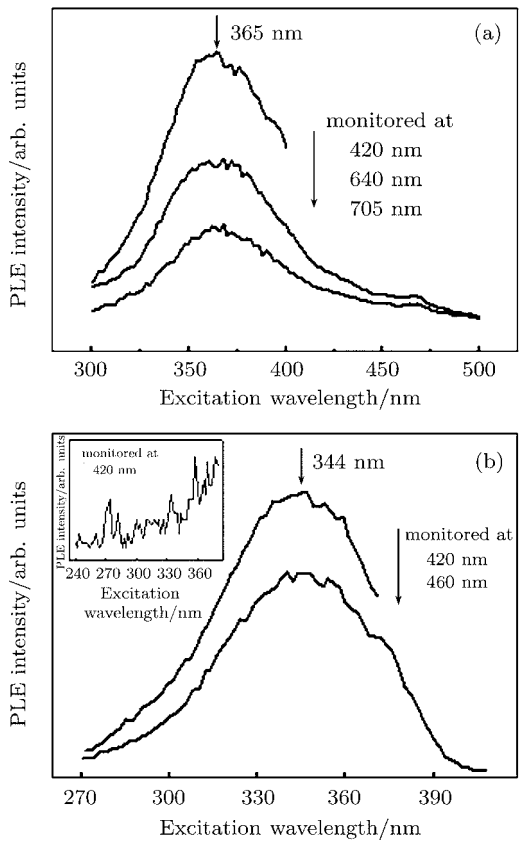


Fig. 5. The PLE spectra of (a) the Si-NPA and (b) the annealed Si-NPA taken under three and two different monitored emission wavelengths, respectively. Inset (b): the PLE spectra of the annealed Si-NPA at 1100 °C for 30 min taken under 410-nm monitored emission wavelength.

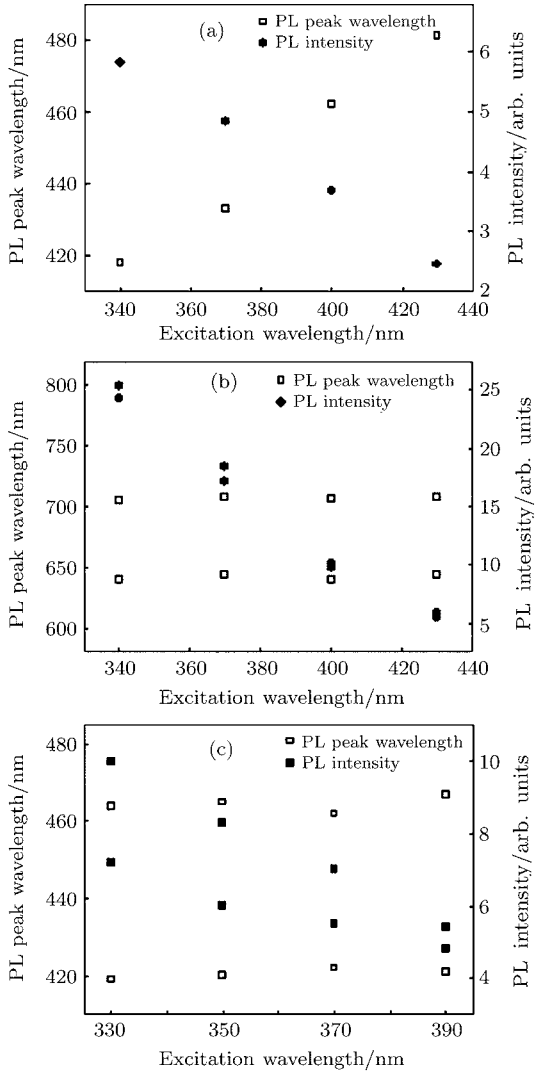


Fig. 6. The PL spectra of the Si-NPA and the annealed Si-NPA measured at different excitation wavelengths: (a) and (b), the PL peak wavelengths and intensities as a function of excitation wavelength for the blue emission band and two red emission bands of th eSi-NPA, respectively; (c) the PL peak wavelengths and intensities as a function of excitation wavelength for two blue emission bands of the annealed Si-NPA.

dence in nc-Si sizes has been widely accepted as an indication of the band–band radiative recombination under the framework of the QC effect.[16,28,29]

(iii) The peak intensities of two red PL bands at 640 nm and 705 nm decrease monotonously with the change of EW from 340 nm to 430 nm, which is similar to the blue PL band, but the peak positions as well as FWHM remain almost unchanged (Fig. 6(b)). This result directly denied the possibility of attributing the origin of the two red PL bands to the pure QC model, because the emission–excitation dependence is thought to be an essential deduction of QC model.[28,29] The PL mechanism of the two red PL bands could be well explained by the QCLC model. According to this model, the excitation process also occurred through the band–band transition in nc-Si, but the emission process mainly occurred through LCs locating at the surface of nc-Si or in the SiO_x layer encapsulating nc-Si.[14,24,30] In the case of Si-NPA, the experimental data of XPS has shown that except the Si atoms in the valence state of Si^{4+}, large quantities of Si atoms are in the valence state of Si^{2+}, and this directly confirmed that two kinds of SiO_x with different x values had been formed because of the different oxidation degrees at different microstructural locations.[14,31,32] This would lead to the formation of two kinds of LCs and therefore two red emission bands were observed.

(iv) The QC and QCLC processes were a pair of competitive photoemission processes and most probably controlled by a critical nc-Si size $L_{\rm m}$, which is ∼2.0 nm for a nanoscale Si/Si oxide systems with the density of LCs $N_{\rm LC} = 10^{15}$ cm^{-3}.[24] For the PL of the Si/Si oxide system, when the size of nc-Si is smaller than $L_{\rm m}$, the QC process plays the major role; while when the size of nc-Si is bigger than $L_{\rm m}$, the QCLC process plays the major role. In the case of the Si-NPA, the nc-Si nanoparticles sized in the range ∼1.95 nm–4.4 nm with an average size of ∼3.4 nm indicate that the majority of nc-Si is bigger than $L_{\rm m}$. This means that the QCLC process would predominate over the PL process of the Si-NPA. The experimental fact that the intensities of the two red PL bands are stronger than that of the blue band is therefore well explained.

The above PL mechanisms for the as-prepared Si-NPA can be sketched effectively via the band energy diagram shown in Fig. 7(a). It is natural to suppose that when the Si-NPA was irradiated by a given EW, only the carriers confined in the nc-Si whose size is bigger than a critical size could be effectively excited. These excited carriers with high energy levels would fall down to the excitation states with relatively low energy levels of nc-Si through some nonradiative recombination process (procedure a in Fig. 7(a)) and then transit back to the ground state through photon emissions (procedure b in Fig. 7(a)). This model well

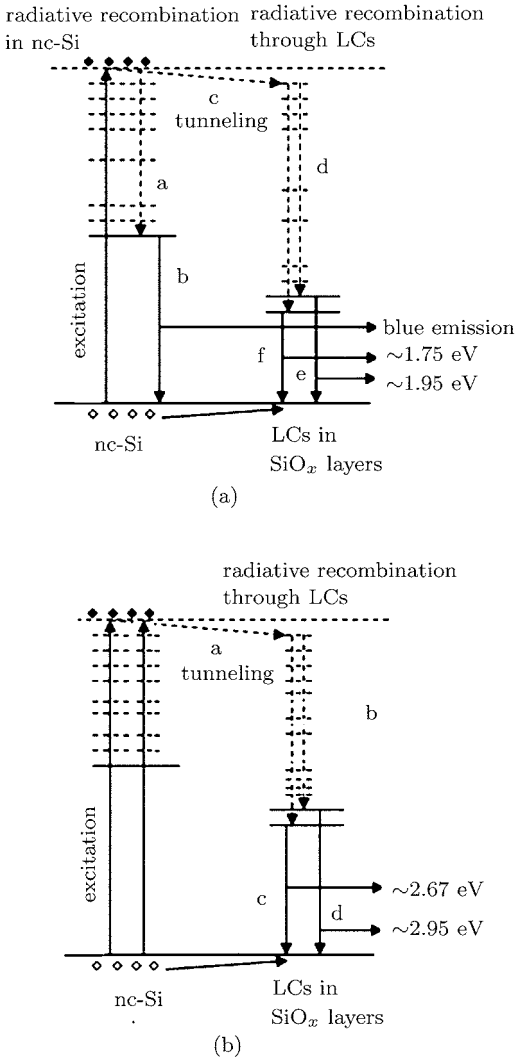


Fig. 7. The schematic representation of the band structure to illustrate the PL mechanisms of the Si-NPA (a) and the annealed Si-NPA (b).

explains the phenomenon of the red shift of the blue emission band in the Si-NPA with increasing EW. Therefore, we tend to conclude that the blue PL in the Si-NPA originates from the QC effect of the carriers confined in variously sized nc-Si. For the QCLC model to explain the two red PL bands, the carriers would firstly transit to the high-energy excitation states of the LCs locating at the surface of nc-Si or in the SiO_x layer encapsulating nc-Si via diffusion or tunneling process (procedure c in Fig. 7(a)), then fall down to

low-energy excitation states of the LCs through some nonradiative recombination process (procedure d in Fig. 7(a)), and finally transit back to the ground state accompanied with photon emissions (procedures e and f in Fig. 7(a)). Since the energy levels of LCs are generally independent of the size of nc-Si, the peak positions of two red emission bands remain unchanged when irradiated by excited light with different wavelengths.

According to the above discussions, the PL mechanism of the two blue PL bands peaking at ∼420 nm and ∼465 nm of the annealed Si-NPA might also be explained by the co-existence of the QC and QCLC effects. Firstly, the PLE spectra of the annealed Si-NPA were also measured by setting the monitoring wavelength at 420 nm and 460 nm, respectively (Fig. 5(b)). It was found that both two PLE spectra exhibit a peak pinned at ∼344 nm, which showed no dependence on the monitored emission wavelength. This result indicates that the carriers for two blue PL bands have the same photoexcited process and strongly suggests that the excitation process for the two blue emission bands might be identical, that is, the photoexcited carriers occur in the nc-Si core. Simultaneously, considering the nc-Si sizes decreased after annealing which have been confirmed from above HRTEM and XRD results, we may easily explain the ∼20 nm blue shift of the PLE peaks (from ∼365 nm for the Si-NPA to ∼344 nm for the annealed Si-NPA). This result not only indicates that the photocexcited process is correlated with the sizes of nc-Si but also further confirms that photoexcited carriers occur in the nc-Si core.

In Fig. 6(c), the PL spectra of the annealed Si-NPA were also measured by using the continuously adjustable monochromatic light as the excitation source. It indicated that the peak intensities of two blue PL bands decrease as EW increases, while the peak positions peaked at ∼420 nm and ∼465 nm remain nearly unchanged, which is similar to that of two red PL bands for the as-prepared Si-NPA. These results reflect that the two blue PL bands of the annealed Si-NPA have similar luminescent origin to the two red PL bands of the Si-NPA and are not sensitive to the nc-Si size, which can be explained by QCLC model.[24,33] Actually, for QC model, increasing EW, we can only excite the electrons and holes in nc-Si units with larger and larger sizes, therefore, the PL peak should have a continuous red-shift, and the FWHM should continuously narrow. But, for two blue PL bands in O_2 ambient annealed Si-NPA, the peak positions and FWHM almost do not change with EW, which further confirm that the PL mechanism of the annealed Si-NPA cannot be explained by QC model. Similar to the origins of two red PL bands for the Si-NPA, using QCLC model and supposing that two kinds of LCs are located at the surfaces of nc-Si units or in SiO_x layers, we can easily explain why the double-peak structures appear in PL spectra and why the positions of two blue PL bands do not change as EW changes. For the disappearance of the PL bands caused by QC effect after annealing, it might be due to the two competitive processes.[33] As being discussed above for the PL mechanisms of Si-NPA, there are two types of photoexcitation–recombination processes for electron–hole pairs: one is that both photoexcitation and recombination occur in nc-Si units as described in QC model, the other is that electrons and holes are photoexcited in nc-Si and recombined through LCs as described in QCLC model. As for the experimental fact that the intensity of two red PL bands is stronger than that of the blue PL band for the Si-NPA, it indicates that the QCLC process would predominate over the QC process. After annealing at 700 °C, the nc-Si sizes have decreased and even disappeared, the quality of the SiO_x layer was improved and the thickness of SiO_x layer was enhanced, which have been proved by FTIR results. This better oxidized surface would form the different LCs and should result in the stronger PL bands relating to the QCLC effect, i.e. the QC effect turned very weak and even disappeared and the QCLC effect was further enhanced. Therefore, for the annealed Si-NPA, the procedures with the photoexicitation occurring in nc-Si just as shown in Fig. 7(b), but the photoemission occurring in different LCs, dominate the PL mechanism (procedures c and d in Fig. 7(b)). In addition, the blue shifts of the PL bands after annealing might attribute to a change of the main LCs from one kind to another and/or the variation of relative contributions from various kinds of LCs.[33] For th eSi-NPA, just as discussed above, two main kinds of LCs came from two kinds of SiO_x oxides with different x values which have been formed because of the different oxidation degree at different microstructure locations. Because of the decrease of nc-Si sizes after annealing, the luminescence energies of the initial main LCs for the Si-NPA are smaller than those of the final main LCs in SiO_x layers for the annealed Si-NPA, and a blue shift will be observed. Furthermore, if we continue the annealing process at 1100 °C for 30 min to make the Si-NPA fully oxidized,

at this point the farther oxidation results in the decrease of the nc-Si sizes or the even complete oxidization of some nc-Si, the PLE peak is not existent when the monitoring wavelength spans at 410 nm (as shown in the inset of Fig. 5(b)), and the blue PL intensity of the Si-NPA turns very weak and even almost disappeares. This result not only ruled out the simple QC model to explain the blue emission process but also explained the weakening QCLC effect because of the almost disappeared photoexicitation occurring in nc-Si.

4. Conclusion

In conclusion, an Si nanocrystal called the Si-NPA was fabricated by hydrothermally etching single crystal Si wafers in hydrofluoric acid containing ferric nitride, which has strong room temperature visible triple-peak PL, one in blue and two in red regions. After annealing of the Si-NPA in O_2 atmosphere at 700 °C for 30 min, only two blue PL bands peaked at ∼420 nm and ∼465 nm were obtained. Spectral analysis indicates that all the photoexcitation processes for three typical emission bands of the Si-NPA and two bands of the annealed Si-NPA are similar, which occurred in nc-Si through a carrier band–band transition process. The different emission bands observed in PL spectra originate from the existence of different recombination paths, band–band recombination for one blue PL band of the Si-NPA, two kinds of LC-band recombination for two red PL bands of the Si-NPA and two blue PL bands of annealed Si-NPA respectively. The clarification on the origin of the different emission bands of the Si-NPA with and without annealing might be important for controlling both the positions and the relative intensities of the PL bands according to future device requirements and further fabricating optoelectronic nanodevices.

References

[1] Ball P 2001 *Nature* **409** 974

[2] Canham L T 1990 *Appl. Phys. Lett.* **57** 1046

[3] Bisi O, Ossicini S and Pavesi L 2000 *Surf. Sci. Rep.* **38** 1

[4] Granitzer P and Rumpf K 2010 *Materials* **3** 943

[5] Urbach B, Axelrod E and Sa'ar A 2007 *Phys. Rev.* B **75** 205330

[6] Stewart M P and Buriak J M 2000 *Adv. Mater.* **12** 859

[7] Lin L, Guo S, Sun X, Feng J and Wang Y 2010 *Nanoscale Res. Lett.* **5** 1822

[8] Smith A, Yamani Z H, Roberts N, Turner J, Habbal S R, Granick S and Nayfeh M H 2005 *Phys. Rev.* B **72** 205307

[9] Ray M, Hossain S M, Klie R F, Banerjee K and Ghosh S 2010 *Nanotechnology* **21** 505602

[10] Bruno M, Palummo M, Marini A, Sole R D and Ossicini S 2007 *Phys. Rev. Lett.* **98** 036807

[11] Peng K Q and Lee S T 2011 *Adv. Mater.* **23** 198

[12] Lin G R, Chang Y C, Liu E S, Kuo H C and Lin H S 2007 *Appl. Phys. Lett.* **90** 181923

[13] Zhang Y H, Li X J, Zhang L and Chen Q W 1998 *Phys. Rev. Lett.* **81** 1710

[14] Xu H J and Li X J 2008 *Opt. Express* **16** 2933

[15] Li P, Wang G, Ma Y and Fang R 1998 *Phys. Rev.* B **58** 4057

[16] Wolkin M V, Jorne J, Fauchet P M, Allan G and Delerue C 1999 *Phys. Rev. Lett.* **82** 197

[17] Godefroo S, Hayne M, Jivanescu M, Stesmans A, Zacharias M, Lebedev O I, Tendeloo G V and Moshchalkov V V 2008 *Nature Nanotechnology* **3** 174

[18] Sato K and Hirakuri K 2006 *J. Vac. Sci. Technol.* B **24** 604

[19] Wang C, Yang Y, Yang R D, Li L, Xiong F and Bao J M 2011 *Chin. Phys.* B **20** 026802

[20] Prokes S M 1993 *Appl. Phys. Lett.* **62** 3244

[21] Wang X X, Zhang J G, Ding L, Cheng B W, Ge W K, Yu J Z and Wang Q M 2005 *Phys. Rev.* B **72** 195313

[22] Delley B and Steigmeier E F 1993 *Phys. Rev.* B **47** 1397

[23] Grosman A, Ortega C, Siejka J and Chamarro M 1993 *J. Appl. Phys.* **74** 1992

[24] Qin G G and Li Y J 2003 *Phys. Rev.* B **68** 085309

[25] Jenkins R and Snyder R L 1996 *Introduction to X-Ray Powder Diffractometry* (New York: Wiley)

[26] Kirk C T 1988 *Phys. Rev.* B **38** 1255

[27] Kamitsos E I 1996 *Phys. Rev.* B **53** 14659

[28] Islam Md N and Kumar S 2003 *J. Appl. Phys.* **93** 1753

[29] Bruno M, Palummo M, Marini A, Sole R D and Ossicini S 2007 *Phys. Rev. Lett.* **98** 036807

[30] Cooke D W, Bennett B L, Famum E H, Hults W L, Sickafus K E, Smith J F, Smith J L, Taylor T N, Tiwari P and Portis A M 1996 *Appl. Phys. Lett.* **68** 1663

[31] Carius R, Fischer R, Holzenkampfer E and Stuke J 1981 *J. Appl. Phys.* **52** 4241

[32] Xu H J and Li X J 2007 *J. Phys.*: *Condens. Matter* **19** 056003

[33] Qin G G, Ran G Z, Sun K and Xu H J 2010 *J. Nanosci. Nanotechnol.* **10** 1584